Framework for the design and analysis of steel fiber reinforced self-compacting concrete structures

A. Orbe, J. Cuadrado*, R. Losada, E. Roji

Construction Engineering Area, Department of Mechanical Engineering, Engineering Faculty of Bilbao, University of the Basque Country (UPV/EHU), Alameda Urquijo, s/n, 48013, Bilbao, Spain

Abstract

This research focuses on the structural applications of steel fiber reinforced concrete (SFRC). Various fibers are first studied, in order to choose the most suitable type in accordance with the specific application. A steel fiber reinforced self-compacting concrete (SFRSCC) mix, designed for improved performance, was used to cast a 3-meter-high, 6-meter-long and 0.15-meter-thick wall. The experimental tests performed on 380 specimens cut from the wall involved mechanical and non-destructive testing (NDT) procedures. Finally, a relationship between magnetic and mechanical properties was established, in order to predict softening and hardening in the flexural behavior of the composite.

Keywords: self-compacting, concrete, fibers, structure, design, control

*Corresponding author
Email address: jesus.cuadrado@ehu.es (J. Cuadrado)

1. Introduction

The use of steel fibers for reinforcing concrete is, at present, generally limited to pavement and tunnel linings. However, many studies have shown that they are suitable for the design of high-performance fiber-reinforced cementitious composites (HPFRCC) [1] or even, engineered cementitious composites (ECC) [2]. Resistance to these products coupled with the difficulties of analyzing fiber distribution and orientation on-site has hindered their entry onto the market.

Different techniques are referred to in the literature to control fiber orientation and content: from the simplest form of manual counting to complex computed tomography (CT) [3][4]. Various image analysis [5] and X-ray methods [6] have been applied, as well as new Non-Destructive Testing (NDT) methods. Among the latter, we may highlight alternate current impedance spectroscopy [7][8], waveguide antennas [9], electrical resistivity measurements [10], open-ended coaxial probe reflectometry methods [11] and magnetic methods [12][13].

Most researchers focus on the study of molded specimens [14][15], which are not representative of real casted structures. They do, however, provide an understanding of the different parameters such as wall effects and the orientation factor [16][17]. At present, there is a huge lack of experience in real-scale structures, with few references in the literature [18][19][20][21].

The selection of the materials is one of the first variables to determine. Several researchers have performed pull-out tests on individual fibers embedded in concrete matrices to study their pull-out mechanisms and them to the macroscopical mechanical properties of the composite[22][23]. However,

there is no agreement on which fiber type might be the most suitable for each application.

Even though information about the influence of matrix strength, fiber geometry, orientation and embedded length in the debonding process and pull-out mechanism of individual fibers can be obtained, it is not suitable for design purposes in structural elements. The randomness of the position and inclination of fibers in a real case, requires regarding the material as a composite, characterized as such.

The addition of fibers to a concrete mix is known to decrease its workability [24]. This has led to new customized mix designs that consider the fibers as new slender aggregates. The aspect ratio of the fibers, grain size and coarse aggregate volume must be limited, in order to avoid fiber balling [5]. Some researchers have verified the suitability of the synergy between steel fiber reinforced concrete and self-compacting concrete technologies [25][26].

The proposed case study analyzes cylindrical retaining walls. Having neither complicated shapes nor congested reinforcement, these walls are quite unlike two-way slabs. Their rebar quantity is oversized for crack control purposes and their low tensile stress means that the rebars may be completely replaced by fibers. This combined with the elimination of vibration can lead to increase the speed and improve the economic efficiency of the construction process. Also labor resources can be optimized and proceed in a better environment with less noise and risks.

Beyond the controlled environment of the laboratory and small-scale studies, this research establishes relevant design and control procedures under real-life building conditions on-site. A large wall made of steel fiber rein-

forced self-compacting concrete (SFRSCC) is casted. The performance of the tank can be assessed characterizing the behavior on multiple specimens, cut from the wall, in ultimate and serviceability limit states. Mechanical properties will be checked by means of compressive, bending and Barcelona tests, while watertightness tests will be held for service conditions. The individual behavior of each specimen was determined and correlated with the global behavior of the element. This approach provides a methodological framework, in order to select the different fiber types and concrete mixtures, test the mechanical properties of the material and provide a reliable method to control fiber distribution and orientation.

2. Materials and mix design

The test fibers shown in Table 1 are typically employed in modern construction processes. Large thick fibers were used in view of the intended structural application.

Fibre Type	HE 1.0/50	HE 1.0/60	Tabix 1.0/50	Tabix 1.0/60
Diameter (mm)	1.0	1.0	1.0	1.0
Length (mm)	50	60	50	60
Geometry	Hooked End		Undulated	
Tensile Strength (MPa)	1100	1450	1100	1450
Aspect Ratio (L/D)	50	60	50	60
Number of fibers per kg	3100	2600	3100	2500

Table 1: Tested steel fibers.

The test program performed 10 pull outs on each fiber type. The fibers were suspended from a foam core board and embedded in mortar. As fibers tend to slip away from the shortest embedded length [27], this was limited to no more than half of the fiber length. The embedded length of the fibers in the test is therefore an average value, a quarter of the fiber length. Steel fixtures were glued to the base of the mortar specimen and the free end of the fibers were fastened with a grip (Figure 1). The test was performed on a Lloyd M5K machine with a capacity of 30KN. A HBM 5KN load cell was used to acquire more accuracy. Load was applied at a displacement rate of 0.5 mm/min up to the maximum load value and at 4 mm/min thereafter. All fibers were aligned with the load direction.

The pull-out behavior of each series reflected a great scattering. The load versus displacement curve can be easily affected by slight changes in the embedded length and inclination. Thus, as above mentioned, individual fiber tests are not suitable for design purposes but provide some information about its debonding behavior. For large embedded lengths, undulated fibers have greater load-bearing capacity than hooked-end fibers, although there is not much difference for short lengths (Figure 2), due to the mechanical component of the pull-out behavior. While undulated fibers need more embedded length to develop all their capability, hooked-end fibers basically only require an embedded hook [28] and longer embedded lengths will not substantially increase the load capacity [29]. Another key point is that undulated fibers tend to straighten out during the test. They therefore attain their maximum load values for larger crack openings. This is not suitable for the proposed application, as it aims to reduce risk of leakage. Therefore, hooked end fibers

were chosen. For the shortest fiber types, hooked-end ones present a lower scattering at maximum load.

Taking account of the proposed application, it is of interest to orient the fibers in a longitudinal direction, which is the direction of maximum tensile stress in a cylindrical tank. This orientation can be achieved with high flowability concrete [30][31]. Mass movement and wall effects help to orient the fibers as intended in this case. Taking fibers as equivalent spherical particles [32], the optimization of the solid skeleton is achieved with less slender aggregates. Shorter fibers will also avoid blockage of the pumping pipe. In view of the above, the chosen fibers are 50 mm long, have a 1 mm diameter hooked-end, and a fiber quantity of 50 kg/m^3. This represents a volume percentage of 0.63, well below the value of 2% that some authors establish for strain hardening behavior [33].

Several mixtures were tested and their fresh concrete properties evaluated with the slump-flow and V-funnel tests. The key issues addressed were segregation resistance, filling ability and passing ability [34]. Passing ability was not essential, because the concrete was not reinforced with rebars. Finally, Table 2 shows the steel fiber reinforced self-compacting concrete (SFRSCC) mix proportion used in the present study. The slump-flow test shows a final diameter (D_f) of 570 mm and a time of 6 seconds to achieve a slump flow of 500 mm (T_{50}). It is a concrete mix with a high yield stress and a low plastic viscosity. Concrete blockage during the V-funnel test meant that it needed 47 seconds to pass through the funnel (T_v). The pumping pipe was the only point where the blockage could feasibly occur. As is well known, pumped concretes behave in different ways in engineering tests [35]. The

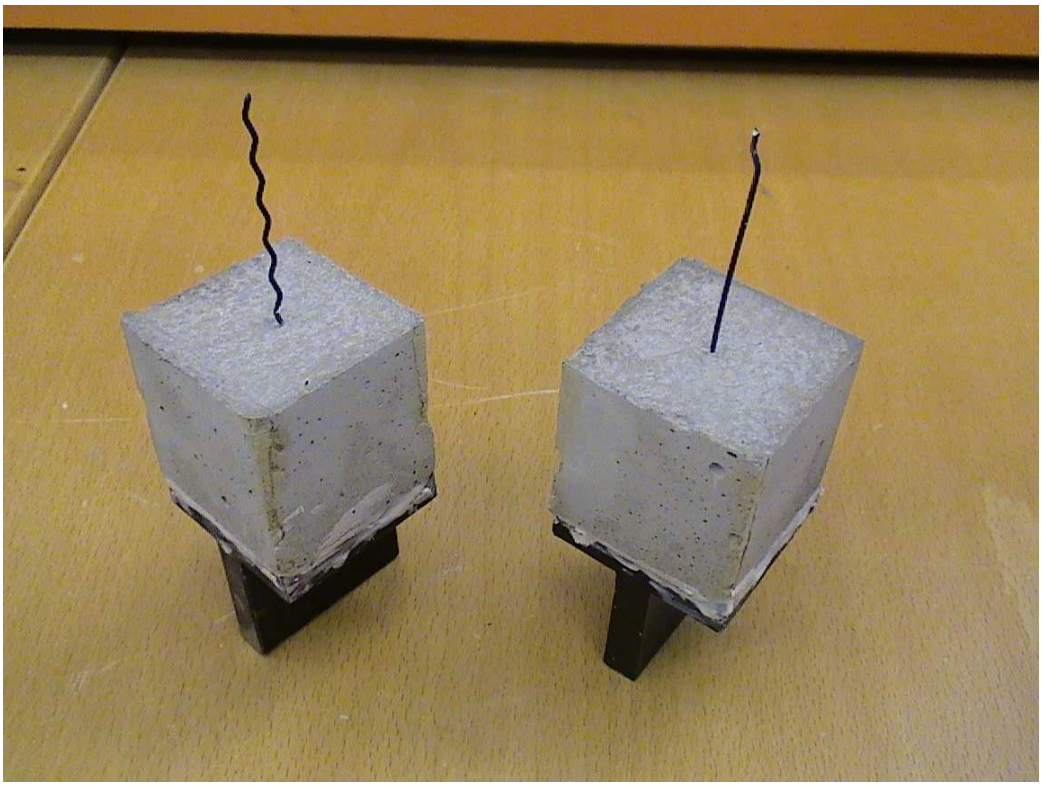

Figure 1: Pull-out tests on undulated (Tabix) and hooked-end (HE) fibers.

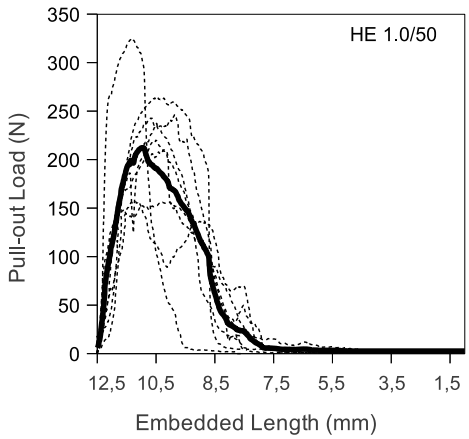

(a) HE 1.0/50

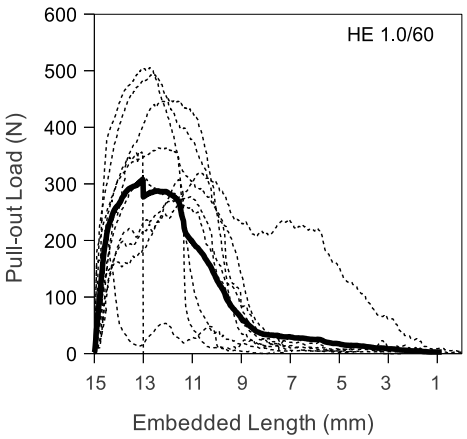

(b) HE 1.0/60

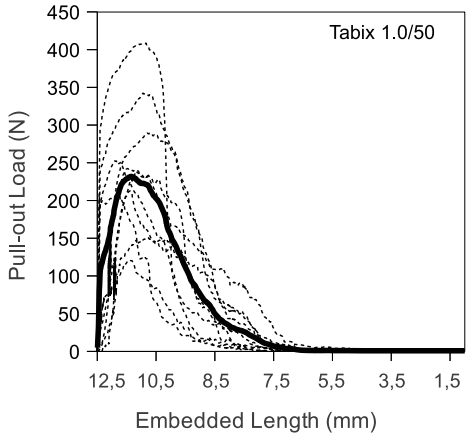

(c) Tabix 1.0/50

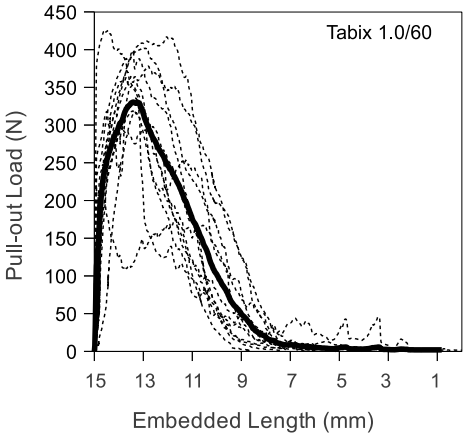

(d) Tabix 1.0/60

Figure 2: Pull-out curves for different fiber types

Materials (kg/m^3)	laboratory	plant
Cement	430	434
Sand (0-4 mm)	1100	1141
Gravel (4-11 mm)	725	626
Plasticizer	4.00	4.43
Superplasticizer	4.80	5.02
Steel fibers	50	50
Water	175	178

Table 2: Steel fiber reinforced self-compacting concrete (SFRSCC) mix-design.

water/cement ratio at 0.41 was low enough to achieve good compactness.

A 4 m^3 batch was prepared, adding the fibers directly to the plant mixer. Notable differences may be seen in the results from the laboratory-level study and from the automated system at the concrete plant, as shown in Table 2. Sand equivalent test and granulometry analysis of aggregates are carried out weekly in the mixing plant. This forced to modify the mix design in order to obtain the maximum compactness of the granular skeleton. Moreover, the slump flow test results varied considerably, obtaining 710 mm and 1.9 seconds for D_f and T_{50} respectively. This could be caused by higher moisture content of aggregates. This could not be properly measured in the absence of a sensor for measuring the moisture of the aggregates in the hoppers. Self-compacting concrete is more sensitive to changes in moisture, which can be controlled better in the laboratory. Short slump times cause uncertainty since it is a visual measurement. In order to obtain better accuracy, recorded

images were edited and T_{50} measured.

3. Experimental program

The mock-up wall was designed also having in mind the subsequent stage of specimen extraction. Mechanical properties were also studied by means of compression (UNE 83507) and Barcelona tests [36] in cubic specimens and a bending test in prismatic specimens (UNE-EN 14651). For one in two rows, three-point bending tests where carried out on the prismatic specimens. The specimens were notched and tested through crack width control. The serviceability of the concrete for structural applications was corroborated by testing the penetration of water under pressure, as per the Spanish Standard UNE-EN 12390-8. Its height was set at 3 meters, its length at 6 meters and thickness at 0.15. The reason for the thinner wall thickness compared with actual structures of this type is that testing standards set that dimension for tested specimens. The concrete was pumped from the bottom left-hand-side corner and it therefore flowed along the formwork to fill up the structure. Figure 3 shows the wall after removal of the formwork. Pumping from one corner was intended to orient the fibers in the direction of mass flow. Information was also obtained on whether the concrete was able to transport the fibers without segregation throughout the formwork. Correct bracing of the formwork and sealing of its joints is very important as the flow of fresh concrete is more fluid and may cause leakage.

Unlike other studies on cast concrete panels, this research does not focus on the overall behavior of the component based on a bending test. On the contrary, 380 specimens were cut and independently analyzed for individual

Figure 3: SFRSCC Wall

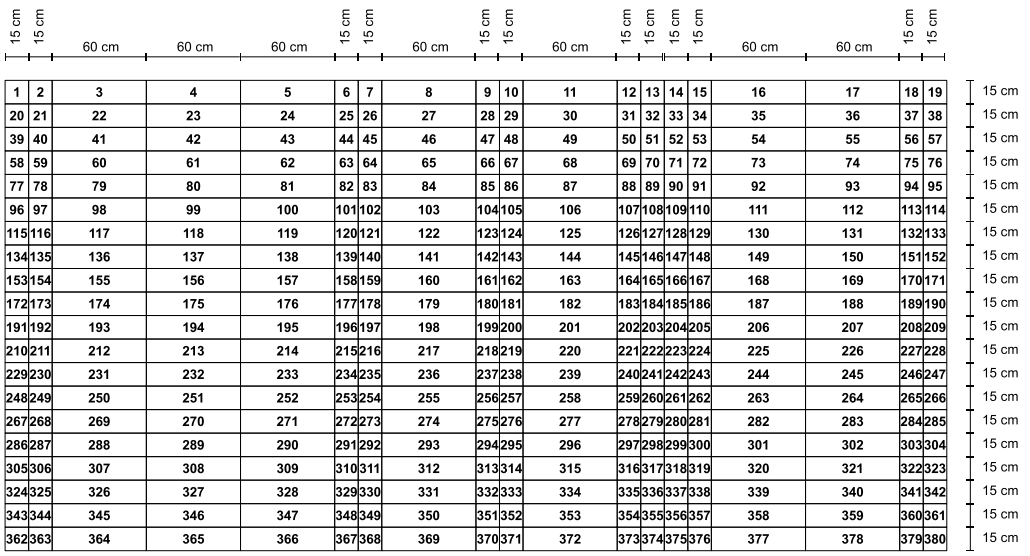

Figure 4: Wall cut scheme.

and global behavior of the element. Different specimen sizes -150 x 150 x 600 mm and 150 x 150 x 150 mm- were cut, as shown in Figure 4. An important point is that the wall did not undergo any curing process, which should help assess its performance under critical conditions.

A manual count of the fibers in the cross sections was performed on each cubic specimen. A bluing technique was applied to the specimens to contrast the concrete and the fibers more sharply by means of surface oxidation, which gave the fibers a darker tonality. Magnetic methods were also applied by means of a continuous uniform coil connected to an Agilent U1732A low-end impedance analyzer (Figure 5). The coil formed of approximately 8800 turns generated a magnetic field with an inductance of 12.3 henrys. Upon introduction of a ferromagnetic material into the coil, the inductance of the magnetic field changes. Three measurements, according to their three main

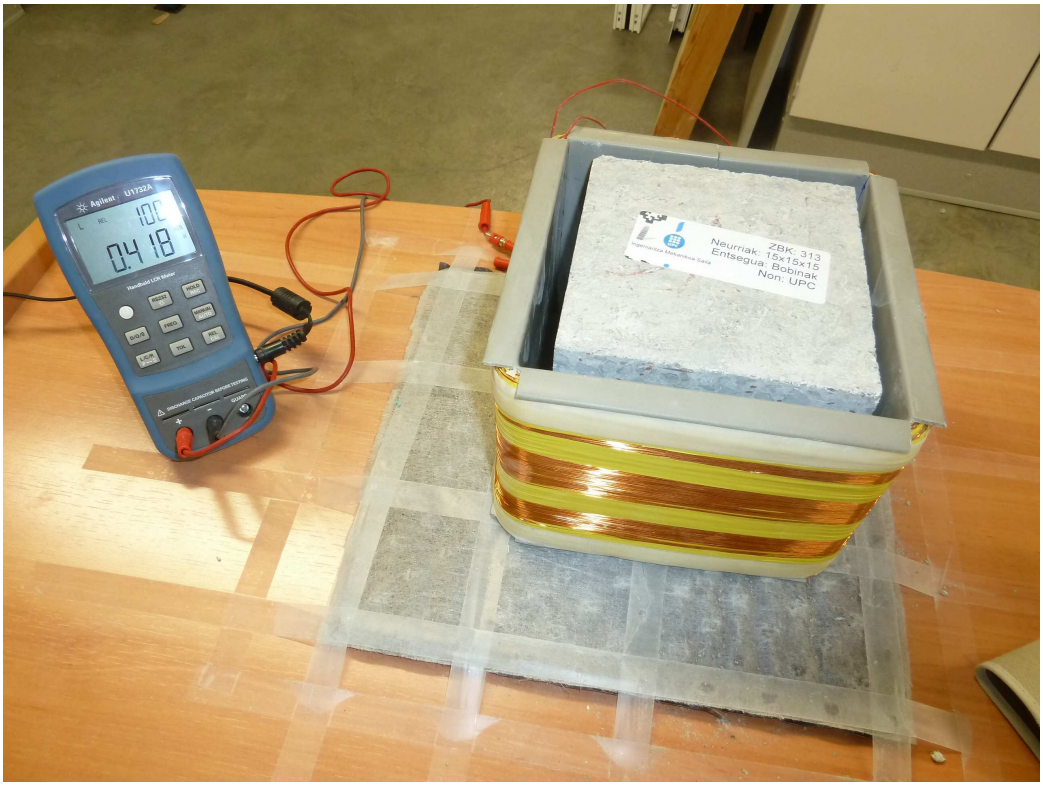

Figure 5: Continuous coil, impedance analyzer and specimen.

axes, were performed on each cubic specimen, after which the average variation value was calculated. The equipment is portable and easily transported on-site. Cubic specimens were crushed after measuring and their fibers manually extracted with the help of a magnet and weighed, in order to verify the accuracy of the method. Moreover, the same magnetic method was applied to the prismatic specimens, but the configuration of the equipment meant that it only measured the inductance variation of the magnetic field that was generated on one axis of the specimen. Measurements were taken along the length of the longitudinal axis at quarterly intervals.

Cores (100 and 50 mm diameter and 150 mm length) were extracted from two specimens and scanned by means of Computer Tomography. This non-destructive analysis is able to provide a view of the fibers throughout the concrete. Images of transverse thin sections of the core were taken every 0.25 mm, while the core was rotating. Subsequent image processing was carried out using three dimensional analysis software. The study provided information on fiber orientation and material porosity. A YXLON Y-CT Compact tomograph located at the University of Burgos was used for these tests.

These tests were jointly conducted at Tecnalia and the Engineering Faculty of Bilbao, by means of a hydraulic test bench (Ibertest Autotest-W with a capacity of 200 KN and 30 KN) and a electromechanical universal testing machine (Sistemas de Ensayo MEM 101 with a loading capacity of 300 KN).

4. Discussion of results

4.1. Non-destructive testing

At first sight, the preferential orientation of the fibers may be observed and an intuitive idea is gained of the different distributions throughout the wall. A light segregation of aggregates occurred due to the priming water of the pump. Nevertheless, this helped obtain a proper calibration curve at different densities within the same element. As shown in figure 6, the fibers tended to orient in horizontal directions along the length of the wall, according to the mass flow. Fewer fibers were observed with a vertical orientation in the horizontal cross-sections.

Figure 6: Number of fibers in horizontal direction (left-hand-side) and vertical direction (right-hand-side).

Manual fiber counts, inductance variation measurements and fiber extraction after crushing were performed consecutively on 20 specimens located in the middle of the wall. The results show the suitability of stereological principles and the accuracy of magnetic methods, as may be seen from Figure 7. It is therefore possible to extrapolate the results and obtain the fiber density for all of the cubic specimens. Except for a few isolated cases, most of the samples show a level that is similar or above the level that is specified in the design phase. The average orientation factor was 0.7, similar to the value that was initially assumed. The highest inductance variation value obtained for the X-axis (Fig. 8), denotes the preferential orientation of the fibers parallel to the mass flow. The smallest numbers of fibers have a transversal alignment across the thickness of the wall, shown on the Y-axis, owing to the effects of the wall and cement flow. It is interesting to denote that in the second quarter from the bottom, the flow has an important vertical component which tend to orient the fibers in that axis (Z) to the detriment of the

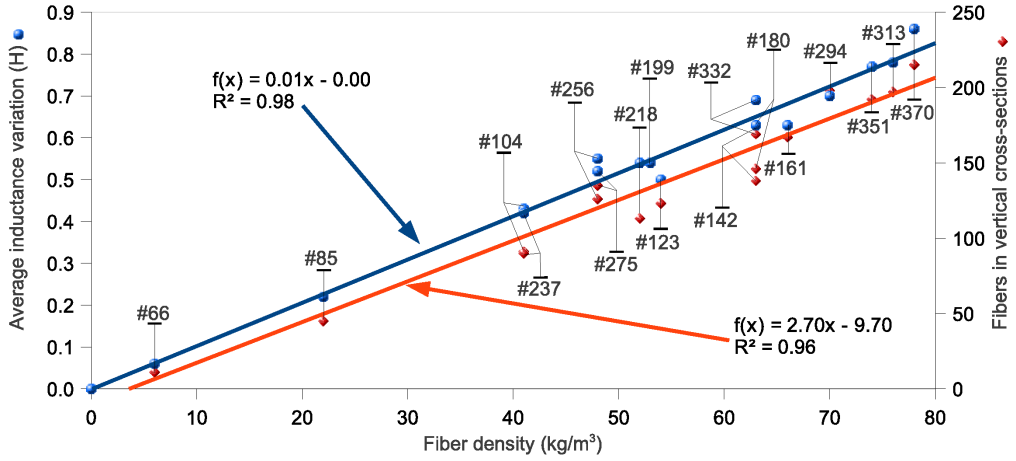

Figure 7: Linearity of stereological and inductive methods for various specimens.

longitudinal (X) one. At the bottom of the wall, vertical flow is small and longitudinal is prevailing. No large variations are observed in the percentage of fibers oriented in Y axis instead.

Tomographic methods applied to the specimens, allow data comparisons to be performed. Figure 9 shows different views of one of the specimens under analysis. The technique provides a view of fiber orientation along the length of the wall, or X-axis, as previous techniques have demonstrated. Table 3 summarizes the total for the projected areas of fibers on the three main axes. Similarly, the predominant orientation is evident. It is an interesting method, but requires specific software for complex post-processing of the images.

Serviceability behavior was tested by studying the penetration of water under pressure in 8 specimens. Correct behavior may be predicted from the data obtained in the tomographic study. The levels of porosity for defects

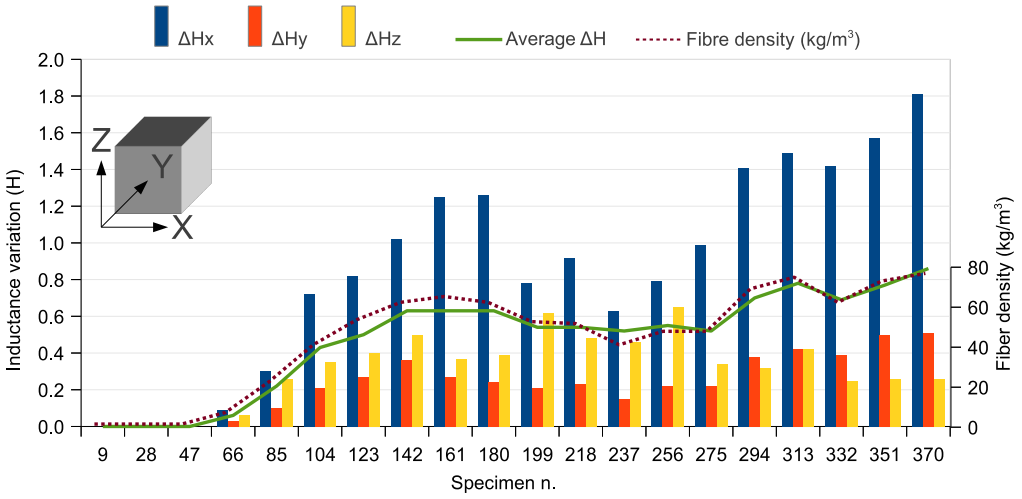

Figure 8: Inductance and average variation for the three axes of the specimen.

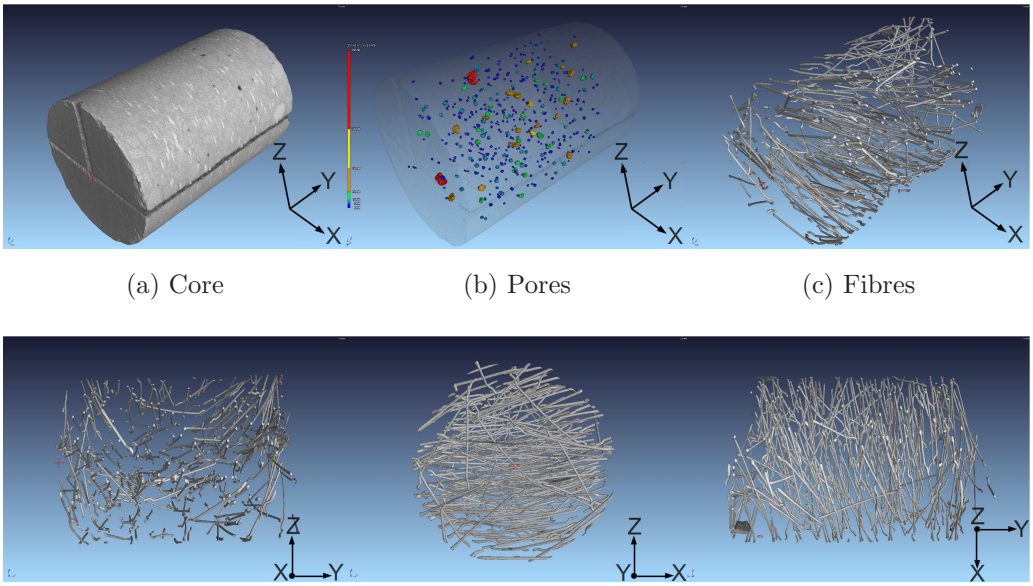

(a) Core (b) Pores (c) Fibres

(d) X axis (e) Y axis (f) Z axis

Figure 9: Core of specimen n.273, isometric image of pore and fiber content, and view from X (longitudinal), Y (transversal) and Z (vertical) axes.

Specimen n.	273	292
Core diameter (mm)	100	50
Core length (mm)	150	150
Σx (mm^2)	5515.73	1513.05
Σy (mm^2)	12665.92	2548.57
Σz (mm^2)	10579.94	2331.72

Table 3: Sum of projected areas of the fibers on the directions of the three axes.

higher than 1 (mm^3), are 0.24% and 0.13% for specimens number 273 and 292, respectively. Such values may be considered small [37]. Maximum water penetration values shown in Figure 10, are concordant with the data given above.

4.2. Mechanical properties

4.2.1. Compression strength

Compression strength is largely conditioned by the requirements imposed at the design stage. The exposure class of this kind of application and its synergy with self-compacting technology, establish a minimum cement dosage that should yield high strength concretes. The compression test was performed on 11 specimens distributed across different parts of the wall (Figure 11). From values resumed in Table 4 an average value of 61 MPa was obtained with a coefficient variation of 9.4%. Further studies may achieve a reduction in that parameter, in order to find applications on elements within a moderate strength range.

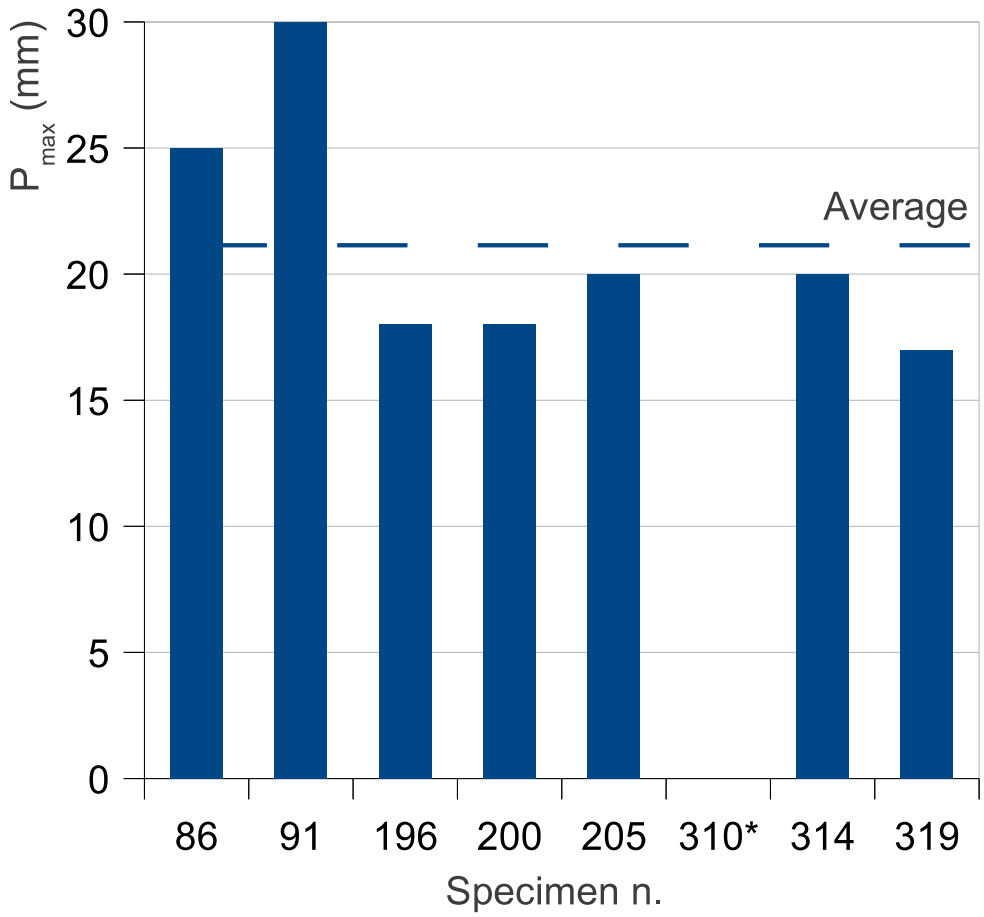

Figure 10: Maximum water penetration values.

Specimen n.	25	29	34	143	148	253	257	262	367	371	376
Compression Strength (MPa)	58.7	55.3	61.0	73.4	64.5	55.7	65.1	66.7	56.6	57.9	56.9

Table 4: Values of compression strength for different specimens.

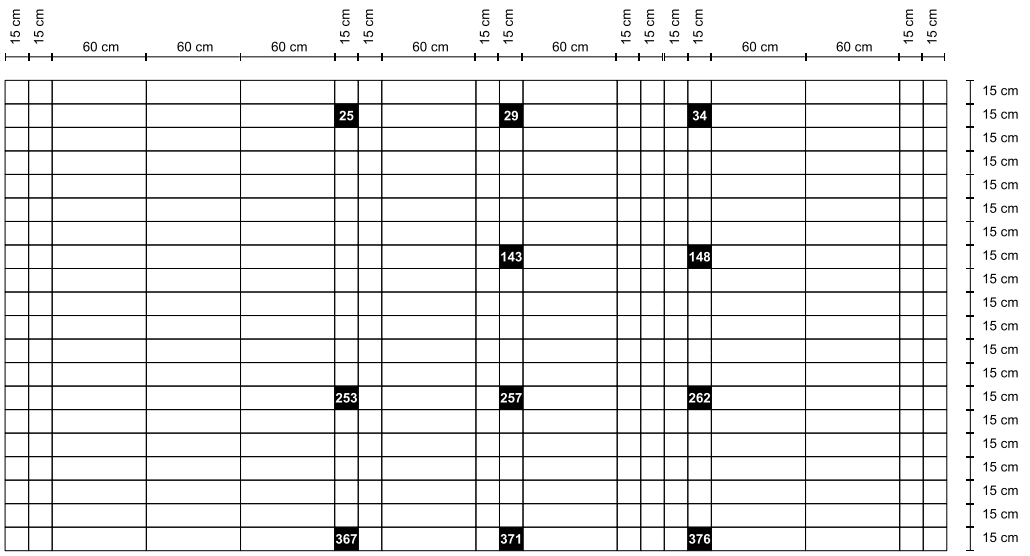

Figure 11: Specimens for compressive test (in black).

As can be observed in Table 4, the height at which the specimen is located does not affect the compression strength. Although fiber density is not measured in those specimens, the values of specimens nearby (Figure 7) show that compression strength is not affected by fiber density.

4.2.2. Barcelona test

The Barcelona test has not been conclusive to establish the real energy absorption capacity of the material. Unlike other experiences [38], only one rupture plane was generated. The 20 specimens (Figure 12) break along the weakest direction (Figure 13), which has hardly no tensile stress as part of the structure. Slip rupture is not fully developed by crack bridging ability of the fibers. The low scattering of maximum values is due to the small contribution of the fibers before concrete cracking. It mainly provides information on concrete matrix strength. In contrast, tenacity depends largely

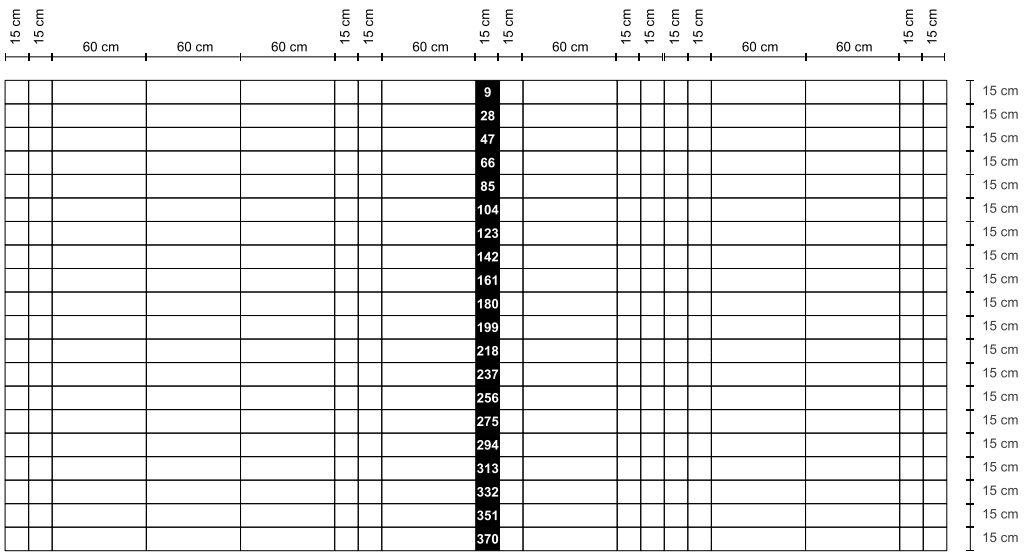

Figure 12: Specimens for Barcelona test (in black).

on the fibers, with greater dispersion according to the different orientations and distributions (Table 5).

Table 5 shows, in accordance to Figure 8, that the fibers tend to align more in transversal direction in specimens at the bottom of the wall. Therefore, the orientation largely affects the tenacity of the material.

4.2.3. Bending test

Contrary to the results of the double punching test, failure occurred along a plane perpendicular to the prevailing direction of the fibers in the 63 bending tests (Figure 14). The material was therefore able to develop its full capacity. The procedure followed, according to UNE-EN 14651, is actually the test recommended by Model Code 2010 for characterization of fiber reinforced concretes (FRC) for structural purposes and identification of relevant parameters to the constitutive relationship to be used in the design phase.

Figure 13: Separation plane in Barcelona test.

Specimen n.	Max. Load (KN)	Tenacity (N*m)	Fibres
370	154.43	297.52	78
351	161.17	232.37	74
332	184.15	206.06	63
313	190.62	324.40	76
294	201.76	339.89	70
275	183.49	264.69	48
256	173.92	182.34	48
237	155.26	161.67	41
218	166.4	162.41	52
199	167,45	190.00	53
180	171.25	215.30	63
161	N/A	N/A	N/A
142	155.15	262.19	63
123	158.13	241.82	54
104	156.59	187.55	41
85	161.67	125.52	22
66	168.86	128.76	6
47	147.3	97.93	0
28	141.73	89.64	0
9	N/A	N/A	N/A

Table 5: Barcelona test results.

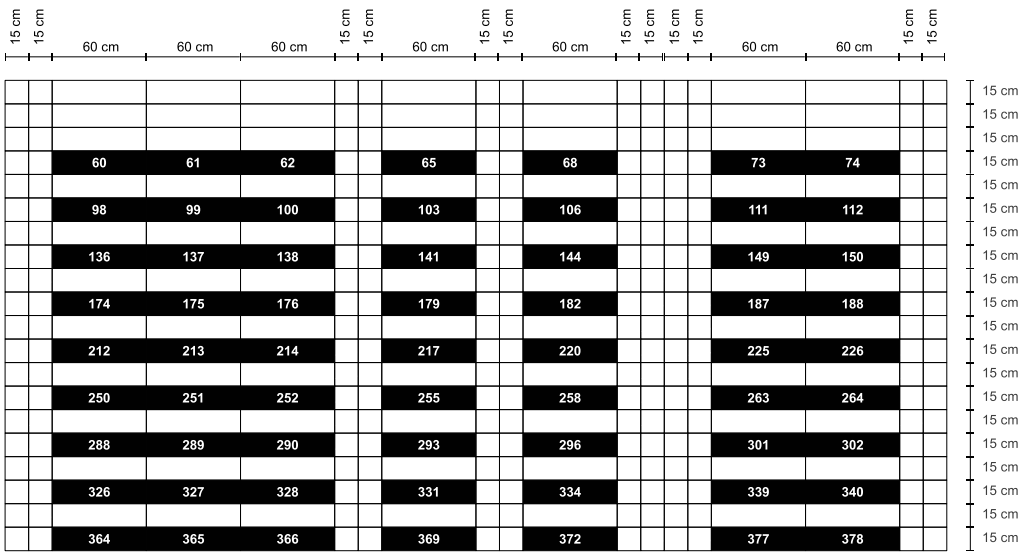

Figure 14: Specimens for Bending test (in black).

Figure 15 shows the mean values of the Limit Of Proportionality (LOP) and residual strengths ($f_{R,i}$) measured for different Crack Opening Mouth Displacements (CMOD = 0.5, 1.5, 2.5 and 3.5 mm, respectively) in the flexure tests. These are plotted alongside the inductance variation on the X axis. The accuracy of the inductive method has been tested in Section 4.1.

As expected, fiber density has little effect on the LOP. On the other hand, residual strengths are a function of the quantity of fibers oriented perpendicular to the rupture plane. The trend lines for residual strengths are parallel to each other and decrease accordingly as the crack openings increase. The scattering of the results, is due to the distribution of fibers across the cross-section, between the compressed zone and tensile zone. The inductive method provides information on the overall orientation of the fibers within the cross section, without particularizing their position (upper or lower

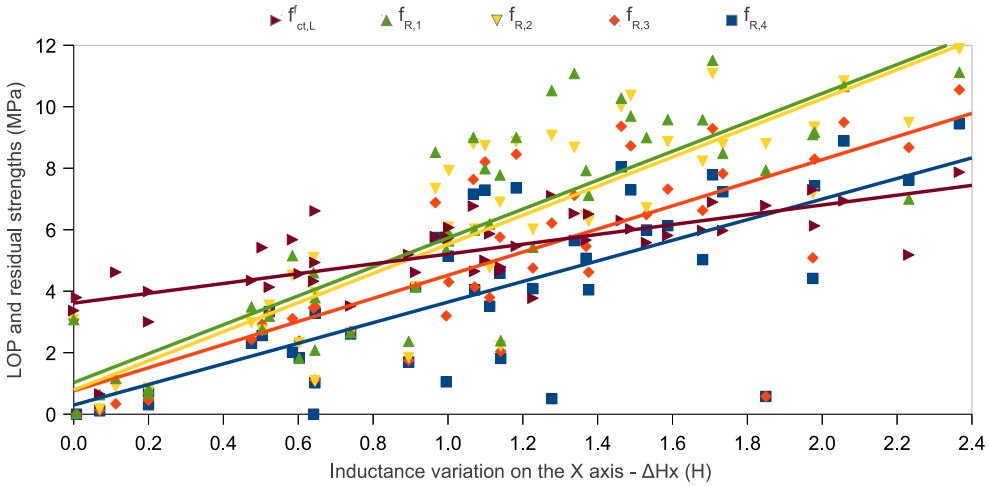

Figure 15: Limit of proportionality $f^{f}_{ct,L}$ and residual strengths in tension in bending $f_{R,1}$, $f_{R,2}$, $f_{R,3}$ and $f_{R,4}$.

zones).

Measurements have been carried out only along the longitudinal axis (X axis), due to the geometric configuration of the coils and specimens. The inductance value represents average measurements in the central section of each specimen (second and third quarters). This measure is increased by the presence of fibers outside the coil that also alter the magnetic field, unlike the cubic specimens that do not protrude from the coil.

Residual strengths are lower for specimens at the left side of the wall. This is due to the short distance the fibers have to cover, so they can not be fully oriented. Also specimens in the right side of the wall show low residual strengths, even thought they flow along all the formwork. The mass movement turns vertical once it reaches the end of the wall. Inductive methods show provide information about the improvement in the material load car-

rying capacity. For inductance variation greater than 0,85 henrys, residual strengths tend to surpass the limit of proportionality. This is also noticeable in the rupture plane of the specimen. A single crack and rupture plane in specimens with low fiber density is obtained and multiple cracks and fracture planes in heavily reinforced ones.

Finally the magnetic method allows us to define a four exponential model [39] that matches the experimentally obtained stress versus CMOD curve. Although the variables are non-physical, one continuously differentiable function is capable of describing the behavior of the material. The main inputs into the model (Eq. 1) are the pre- and post-cracking maximum stresses (usually $f^{f}_{ct,L}$ and $f_{R,1}$) and their respective crack mouth opening displacements.

$$f(x) = c_1(e^{-c_2 x} - e^{-c_3 x}) + c_4(e^{-c_5 x} - e^{-c_6 x}) \tag{1}$$

The constants c_1, c_2, c_3, c_4, c_5 and c_6 (Eq. 2 to 7) depend on the shape parameters α_1 and α_2. Values 1.001 and 100 are suitable for the specimens which best suit the regression equations.

$$c_1 = \frac{f_{max,pre-cracking}}{\left(\alpha_1^{\frac{1}{1-\alpha_1}} - \alpha_1^{\frac{\alpha_1}{1-\alpha_1}} \right)} \tag{2}$$

$$c_2 = \frac{ln\alpha_1}{x_{max,pre-cracking}(\alpha_1 - 1)} \tag{3}$$

$$c_3 = \alpha_1 c_2 \tag{4}$$

$$c_4 = \frac{f_{max,post-cracking}}{\left(\alpha_2^{\frac{1}{1-\alpha_2}} - \alpha_2^{\frac{\alpha_2}{1-\alpha_2}} \right)} \tag{5}$$

$$c_2 = \frac{ln\alpha_2}{x_{max,post-cracking}(\alpha_2 - 1)} \tag{6}$$

$$c_6 = \alpha_2 c_5 \tag{7}$$

The validity of the model was tested by comparing the values actually obtained in bending tests and the predicted values, applying the four exponential model to inductance variation measures, which were in turn calculated from regressions equations (8) and (9). The input parameters are given in Table 6.

$$P_{max,pre-cracking} = 1.6\Delta H + 3.61 \tag{8}$$

$$P_{max,post-cracking} = 4.7\Delta H + 1.03 \tag{9}$$

In cylindrical retaining walls, the main tensile stress is located along the perimeter. Its value is obtained according to the symmetric deformation theory in circular cylindrical plates [40]. As an example, a 4-meter-high, 10-meter-diameter wall with a thickness of 0.25 meter that is hinged at the base, has a maximum tensile force of 132.56 KN located at a third of the height. It corresponds to low service stresses, close to 0.5 MPa. The tensile strengths of the tested specimens are well over this value.

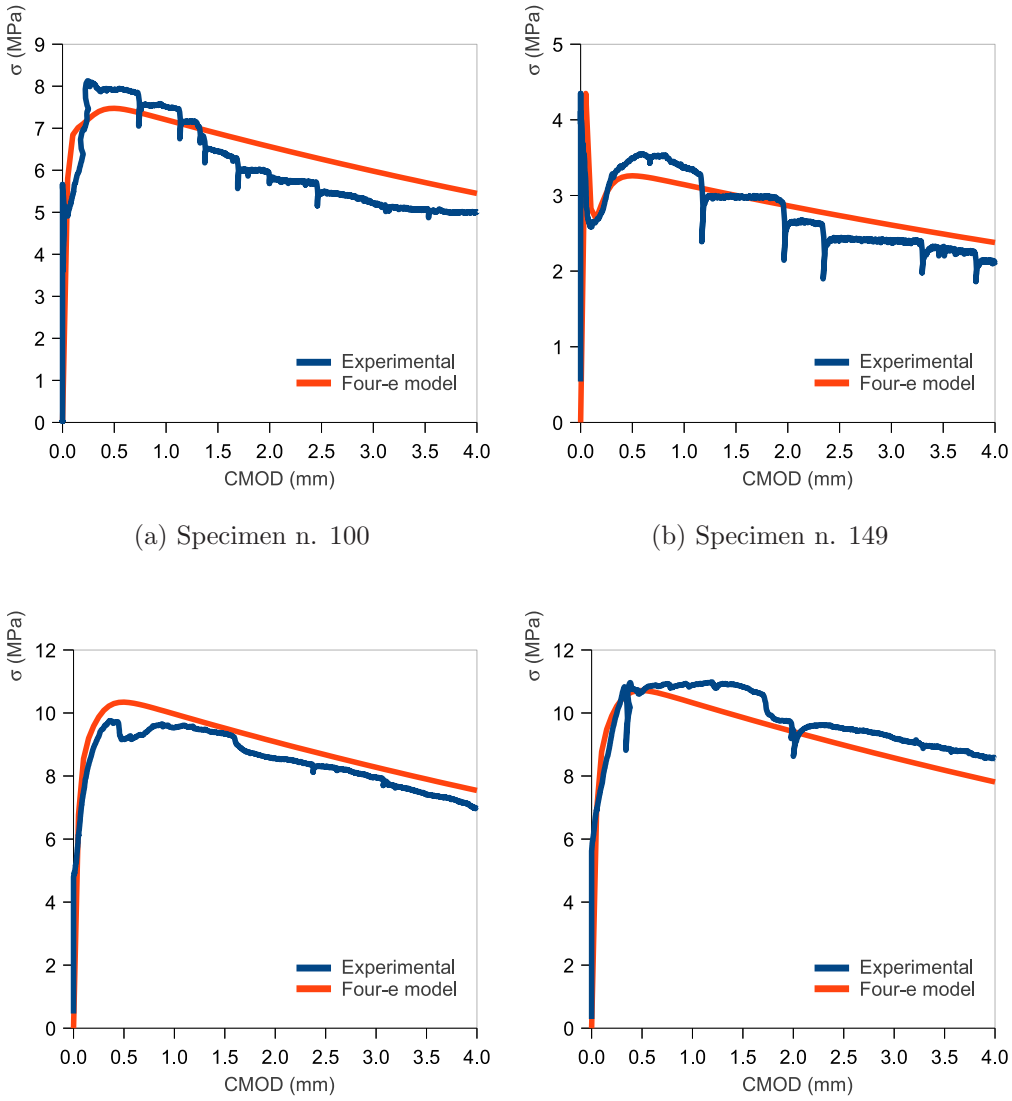

(a) Specimen n. 100

(b) Specimen n. 149

(c) Specimen n. 296

(d) Specimen n. 301

Figure 16: Four exponential model and bending test results.

Specimen n.	100	149	296	301
Inductance variation (ΔH)	1.369	0.475	1.980	2.058
$P_{max,pre-cracking}$ (MPa)	5.66	4.37	6.77	6.90
$x_{max,pre-cracking}$ (mm)	0.05	0.024	0.05	0.05
$P_{max,post-cracking}$ (MPa)	7.92	3.26	10.34	10.71
$x_{max,post-cracking}$ (mm)	0.5	0.5	0.5	0.5

Table 6: Four exponential model input parameters.

5. Conclusions

The paper has presented a methodological framework for the design of SFRSCC and its analysis in a structural application of the industrial sector. Fiber reinforced and self-compacting technologies are merged for optimum performance in circular retaining walls. Once structural behavior is known by means of classical structural analysis tools, most suitable fiber type and mix design are chosen. The structural safety is verified testing specimens cut from a real-scale wall, unlike other studies which are based on molded specimens. In addition to the load-carrying capacity provided by the fibers, serviceability and watertightness are also guaranteed.

Mechanical properties are correlated with results obtained from non-destructive tests. This tests allow to establish a constitutive relation between strengths and fiber dispersion, depending on the casting process, for design purposes. Also inductive methods show adequate for checking its proper performance at the structural level.

Acknowledgements

The authors gratefully acknowledge the support obtained from the Spanish Ministry of Science and Innovation and the Regional Government of Biscay through MIVES IV ref: BIA 2010-20789-C04-04 and BIRGAITEK 7-12-TK-2009-10 grants, respectively. The first author also gratefully acknowledges the participation of Tecnalia, ArcelorMittal-Wire Solutions and Financiera y Minera (Italcementi Group) in the experimental phase and shows his appreciation to Antonio Aguado, Josep Maria Torrents, Ana Blanco and Pablo Pujadas for their support.

References

[1] Wille, K., Kim, D.J., Naaman, A.E.. Strain-hardening uhp-frc with low fiber contents. Materials And Structures 2011;44(3):583–598.

[2] Sahmaran, M., Li, V.C.. Engineered cementitious composites can composites be accepted as crack-free concrete? Transportation Research Record 2010;2164(2164):1–8.

[3] Stähli, P., Custer, R., van Mier, J.. On flow properties, fibre distribution, fibre orientation and flexural behaviour of frc. Materials and Structures 2008;41:189–196. 10.1617/s11527-007-9229-x.

[4] Barnett, S.J., Lataste, J.F., Parry, T., Millard, S.G., Soutsos, M.N.. Assessment of fibre orientation in ultra high performance fibre reinforced concrete and its effect on flexural strength. Materials and Structures 2010;43:1009–1023. 10.1617/s11527-009-9562-3.

[5] Grünewald, S.. Performance-based design of self-compacting fibre reinfroced concrete. Ph.D. thesis; Technische Universiteit Delft; 2004.

[6] Robins, P., Austin, S., Jones, P.. Spatial distribution of steel fibres in sprayed and cast concrete. Magazine Of Concrete Research 2003;55(3):225–235.

[7] Ozyurt, N., Mason, T.O., Shah, S.P.. Non-destructive monitoring of fiber orientation using ac-is: An industrial-scale application. Cement and Concrete Research 2006;36(9):1653 – 1660.

[8] Ozyurt, N., Woo, L.Y., Mason, T.O., Shah, S.P.. Monitoring fiber dispersion in fiber-reinforced cementitious materials: Comparison of ac-impedance spectroscopy and image analysis. ACI Materials Journal 2006;103(5):340–347.

[9] Roqueta, G., Jofre, L., Romeu, J., Blanch, S.. Broadband propagative microwave imaging of steel fiber reinforced concrete wall structures. Instrumentation and Measurement, IEEE Transactions on 2010;59(12):3102 –3110.

[10] Lataste, J., Behloul, M., Breysse, D.. Characterisation of fibres distribution in a steel fibre reinforced concrete with electrical resistivity measurements. NDT & E International 2008;41(8):638 – 647.

[11] Van Damme, S., Franchois, A., Taerwe, L.. Comparison of two coaxial probes for the non-destructive evaluation of a steel fiber reinforced concrete layer. In: Proc. 21st IEEE Instrumentation and Measurement Technology Conf. IMTC 04; vol. 1. 2004, p. 579–582.

[12] Blanco, A., Pujadas, P., Aguado, A., Torrents, J.M.. Método inductivo para evaluar cuantía y orientación de fibras de acero en hormigón. In: científico-técnica del hormigón estructural, A., editor. V Congreso de ACHE. Asociación científico-técnica del hormigón estructural; 2011, p. 285–286.

[13] Faifer, M., Ottoboni, R., Toscani, S., Ferrara, L.. Nondestructive testing of steel-fiber-reinforced concrete using a magnetic approach. Instrumentation and Measurement, IEEE Transactions on 2011;60(5):1709 –1717.

[14] Gettu, R., Gardner, D., Saldivar, H., Barragan, B.. Study of the distribution and orientation of fibers in sfrc specimens. Materials And Structures 2005;38(275):31–37.

[15] Barros, J., Cunha, V., Ribeiro, A., Antunes, J.. Post-cracking behaviour of steel fibre reinforced concrete. Materials and Structures 2005;38:47–56.

[16] Stroeven, P., Hu, J.. Effectiveness near boundaries of fibre reinforcement in concrete. Materials and Structures 2006;39:1001–1013. 10.1617/s11527-006-9101-4.

[17] Dupont, D., Vandewalle, L.. Distribution of steel fibres in rectangular sections. Cement and Concrete Composites 2005;27(3):391 – 398.

[18] Maturana, A., Sanchez, R., Canales, J., Orbe, A., Ansola, R.,, , et al. Technical-economic analysis of steel fibre reinforced concrete flag slabs.

a real building application. In: Proceedings pf XXXVII IAHS World Congress of Housing. 2010, p. 119.

[19] Serna, P., Arango, S., Ribeiro, T., Núez, A., Garcia-Taengua, E.. Structural cast-in-place sfrc: technology, control criteria and recent applications in spain. Materials and Structures 2009;42:1233–1246.

[20] Michels, J., Waldmann, D., Maas, S., Zuerbes, A.. Steel fibers as only reinforcement for flat slab construction - experimental investigation and design. Construction And Building Materials 2012;26(1):145–155.

[21] Destrée, X.. Concrete free suspended elevated slabs reinforced with only steel fibers: Full scale testing results and conclusions - design examples. In: Fischer, G., Li, V.C., editors. Book title: International RILEM Workshop on High Performance Fiber Reinforced Cementitious Composites in Structural Applications. RILEM; RILEM Publications SARL; 2006, p. 287 – 294.

[22] Cunha, V.M.C.F.. Steel fibre reinforced self-compacting concrete (from micromechanics to composite behavior). Ph.D. thesis; Universidade do Minho, Departamento de Engenharia Civil, Azurém, 4800-058 Guimaraes, Portugal; 2010.

[23] Robins, P., Austin, S., Jones, P.. Pull-out behaviour of hooked steel fibres. Materials and Structures 2002;35:434–442. 10.1007/BF02483148.

[24] Swamy, R.. Fibre reinforcement of cement and concrete. Materials and Structures 1975;8:235–254. 10.1007/BF02475172.

[25] Ferrara, L., Tregger, N., Shah, S.P.. Flow-induced fiber orientation in scsfrc: Monitoring and prediction. In: Khayat, K.H., Feys, D., editors. Design, Production and Placement of Self-Consolidating Concrete; vol. 1 of RILEM Bookseries. Springer Netherlands; 2010, p. 417–428.

[26] Torrijos, M.C., Barragán, B.E., Zerbino, R.L.. Placing conditions, mesostructural characteristics and post-cracking response of fibre reinforced self-compacting concretes. Construction and Building Materials 2010;24(6):1078 – 1085.

[27] Li, V.C., Wang, Y., Backer, S.. A micromechanical model of tension-softening and bridging toughening of short random fiber reinforced brittle matrix composites. Journal of the Mechanics and Physics of Solids 1991;39(5):607 – 625.

[28] Laranjeira, F., Molins, C., Aguado, A.. Predicting the pullout response of inclined hooked steel fibers. Cement And Concrete Research 2010;40(10):1471–1487.

[29] Cunha, V.M.C.F., Barros, J.A.O., Sena-Cruz, J.M.. Pullout behavior of steel fibers in self-compacting concrete. Journal of Materials in Civil Engineering 2010;22(1):1–9.

[30] Boulekbache, B., Hamrat, M., Chemrouk, M., Amziane, S.. Flowability of fibre-reinforced concrete and its effect on the mechanical properties of the material. Construction And Building Materials 2010;24(9):1664–1671.

[31] Ferrara, L., Ozyurt, N., di Prisco, M.. High mechanical performance of fibre reinforced cementitious composites: the role of "casting-flow induced" fibre orientation. Materials And Structures 2011;44(1):109–128.

[32] Ferrara, L., Park, Y.D., Shah, S.P.. A method for mix-design of fiber-reinforced self-compacting concrete. Cement and Concrete Research 2007;37(6):957 – 971.

[33] Fantilli, A.P., Mihashi, H., Vallini, P.. Multiple cracking and strain hardening in fiber-reinforced concrete under uniaxial tension. Cement and Concrete Research 2009;39(12):1217 – 1229.

[34] Okamura, H., Ouchi, M.. Self-compacting concrete. Journal of advanced concrete technology 2003;1(1):5–15.

[35] Zerbino, R., Barragán, B., Garcia, T., Agulló, L., Gettu, R.. Workability tests and rheological parameters in self-compacting concrete. Materials and Structures 2009;42:947–960. 10.1617/s11527-008-9434-2.

[36] Molins, C., Aguado, A., Saludes, S.. Double punch test to control the energy dissipation in tension of frc (barcelona test). Materials And Structures 2009;42(4):415–425.

[37] Bermejo Núñez, E.B., Moragues Terrades, A., Gálvez Ruíz, J., Fernández Cánovas, M.. Permeability and pore size distribution in medium strength self-compacting concrete. Materiales de Construcción 2010;60(299):37–51.

[38] Pujadas, P., Blanco, A., Cavalaro, S.H.P., Aguado, A.. Método para la caracterización multidireccional del hrf. In: científico-técnica del hormigón estructural, A., editor. V Congreso de ACHE. Asociación científico-técnica del hormigón estructural; 2011, p. 289–290.

[39] Lee, M., Barr, B.. A four-exponential model to describe the behaviour of fibre reinforced concrete. Materials and Structures 2004;37:464–471. 10.1007/BF02481583.

[40] Timoshenko, S., Woinosky-Krieger, S.. Theory of plates and shells. New York: McGraw-Hill; 1959.